Electronic Supplementary Material (ESI) for Physical Chemistry Chemical Physics.

This version of the ESI replaces the one published on 17.01.2020 as the previous version had errors in the data

Benchmark and application of long-range corrected time-dependent density functional tight binding (LC-TD-DFTB) on rhodopsins and light-harvesting complexes: Supplementary material

Beatrix M. Bold,[1] Monja Sokolov,[1] Sayan Maity,[2] Marius Wanko,[3] Philipp M. Dohmen,[1] Julian J. Kranz,[1,4] Ulrich Kleinekathöfer,[2] Sebastian Höfener,[1] and Marcus Elstner[1,4]

[1]*Institute of Physical Chemistry, Karlsruhe Institute of Technology (KIT), Kaiserstrasse 12, 76131 Karlsruhe, Germany*

[2]*School of Science, Constructor University, Campusring 1, 28759 Bremen, Germany*

[3]*Nano-Bio Spectroscopy Group and ETSF, Dpto. Material Physics, Universidad del País Vasco, 20018 San Sebastián, Spain*

[4]*Institute of Biological Interfaces (IBG2), Karlsruhe Institute of Technology (KIT), Kaiserstrasse 12, 76131 Karlsruhe, Germany*

PLEASE NOTE

This corrected Supporting Information contains still old values, which were not recalculated: Table S6 (LC-DFTB Coulomb couplings), Table S11, S12 and S15 (ring system LC-DFTB), Table S13 and S16 (both columns), Table S14 (LC-DFTB Coulomb couplings), Table S18 (coupled chromophores LC-DFTB); Figs. S9, S10, S11.

Corrected values are shown in Tables S17, S19, S20 and S21 and Figs. S5, S7 and S8.

S-1. COMPUTATIONAL DETAILS

S-1.1. Equilibration and classical MD simulation of the LH complexes

The LH2 complex was minimized using the steepest descent algorithm (max. 50000 steps with a tolerance of 1000 kJ mol^{-1} nm^{-1}). Subsequently, the system was equilibrated for 3 ns at a temperature of 300 K using the Nosé-Hoover thermostat [1, 2] with a time step of 1 fs. During this step, the heavy atoms of the protein and all chromophores have been restrained to their initial positions by harmonic potentials (force constant: 1000 kJ mol^{-1} nm^{-1}). In addition, an NPT equilibration was performed with a length of 8 ns and a pressure of 1 bar using the Parrinello-Rahman barostat [3] and a time step of 2 fs. Subsequently, the restraints were removed and an NPT equilibration of 1 ns was performed. After the equilibration, the LH2 complex has been simulated for 1 ns.

As for the LH2 complexes, also for the simulations of the FMO complex, periodic boundary conditions were applied and long-range interactions were determined using the Particle-Mesh Ewald method. The FMO complex has been equilibrated in the same way as the LH2 complex. The NVT equilibration was performed with a length of 1 ns and the NPT equilibration with a length of 5 ns. The production run performed at 300 K, had a length of 100 ns with a timestep of 1 fs. From the 100 ns MD trajectory, 1 ns was taken to generate the sampled structures for the computation of the excitation energies and Coulomb couplings.

S-1.2. Excitonic Coupling

In the supermolecular approach, both the Coulombic and exchange interaction are considered by default. The Frenkel Hamiltonian for a two level donor and acceptor system can

be written as

$$H_{mn} = \begin{pmatrix} E_m & V_{mn} \\ V_{nm} & E_n \end{pmatrix} . \tag{1}$$

In this expression, $E_{m,n}$ denote the excitation energies for the individual monomer and V_{mn} the excitonic coupling. For identical donor and acceptor molecules, i.e., if $E_m = E_n$ are equal, the eigenvalues are given by $\lambda_{1,2} = \frac{1}{2}(E_1 - E_2)$, where E_1 and E_2 are the two lowest excitonic energies in a supermolecular framework [4, 5].

For chromophores which are well separated the excitonic coupling can be estimated accurately by calculating the Coulomb coupling only, since the exchange part decays exponentially with distance. One way to accurately calculate the Coulomb coupling is the TrESP approach (transition charges by electrostatic potential). In this approach, the molecular transition density of each individual molecule is fitted by so-called atomic transition charges q_i^T. The coupling can be subsequently determined using [6, 7]

$$V_{mn} = \frac{1}{4\pi\epsilon_0} \sum_{i,j=1}^{m,n} \frac{q_i^T q_j^T}{\mid r_i - r_j \mid} . \tag{2}$$

In LC-DFTB, the computation of Coulomb couplings in a spirit of Mulliken transition charges is based on DFTB2 with the time-dependent extension. The Coulomb couplings V_{mn} are obtained using

$$V_{mn} = \sum_{a,b=m,n} Q_a Q_b \gamma_{ab} \tag{3}$$

where Q_a and Q_b denote the Mulliken transition charges and where the γ-function describes the second-order Coulomb interaction. Following the scheme of Ref. [8], the approach was extended using LC-DFTB. The advantages of computing Coulomb couplings in the spirit of DFTB is given by the transition charges, which can be calculated "on the fly" along a MD trajectory but depends on the accuracy of the DFTB method.

S-2. BENCHMARK

S-2.1. Retinal

Tab. S1: Excitation energies (eV) of all-*trans* retinal geometries optimized in vacuum using different methods. Bond length alternation (BLA) is given in Å.

	CASSCF	HF	BH-LYP	B3LYP	DFTB	BLYP
BLA[a]	0.100	0.069	0.035	0.028	0.025	0.023
SORCI[a]	2.10	2.07	2.04	1.95	1.91	1.89
ZINDO/S	2.36	2.38	2.33	2.28	2.25	2.24
CAM-B3LYP	2.68	2.77	2.80	2.76	2.69	2.68
LC-BLYP	2.75	2.76	2.70	2.62	2.57	2.56
ωB97X	2.82	2.82	2.76	2.67	2.62	2.61
LC-DFTB	2.63	2.69	2.69	2.60	2.57	2.55
ADC(2)	1.94	2.01	2.03	1.93	1.89	1.87
SOS-ADC(2)	2.32	2.28	2.20	2.08	2.05	2.01

[a] Taken from Ref. 9.

1. *Twist of β-ionone ring*

Tab. S2: Excitation energies (eV) of a 6-s-cis-11-cis PSB in vacuum for different twist angles of the β-ionone ring.

	33°	60°	90°	171°
SORCI[a]	1.96	1.99	2.28	1.95
ZINDO/S	2.32	2.40	2.58	2.27
CAM-B3LYP	2.68	2.66	3.08	2.70
LC-BLYP	2.63	2.70	2.94	2.60
WB97X	2.69	2.77	3.00	2.66
LC-DFTB	2.59	2.57	2.94	2.59
ADC(2)	1.94	2.03	2.27	1.92
SOS-ADC(2)	2.15	2.26	2.40	2.08

[a] Taken from Ref. 9.

2. *Potential energy surface (PES)*

LC-DFTB is benchmarked for the description of the potential energy surface (PES) from the 6-s-*cis*-11-*cis* PSB to a 6-s-*trans*-11-*cis* PSB configuration. The ground state pathway is taken, optimized with PBE0 and the energy profiles of the first two excited states are calculated using LC-DFTB. Fig. S1 compares LC-DFTB with CC2 results from Ref. [10], where the same optimized geometries were used. LC-DFTB describes the PES qualitatively correct when compared to the CC2 results. Similar results have been obtained for the CAM-B3LYP functional (data not shown), which corrects the wrong behavior of B3LYP displaying a red shift of the potential energy surface of the first excited state [10]. This failure of standard TD-DFT functionals can be seen also for TD-DFTB in Fig. S1.

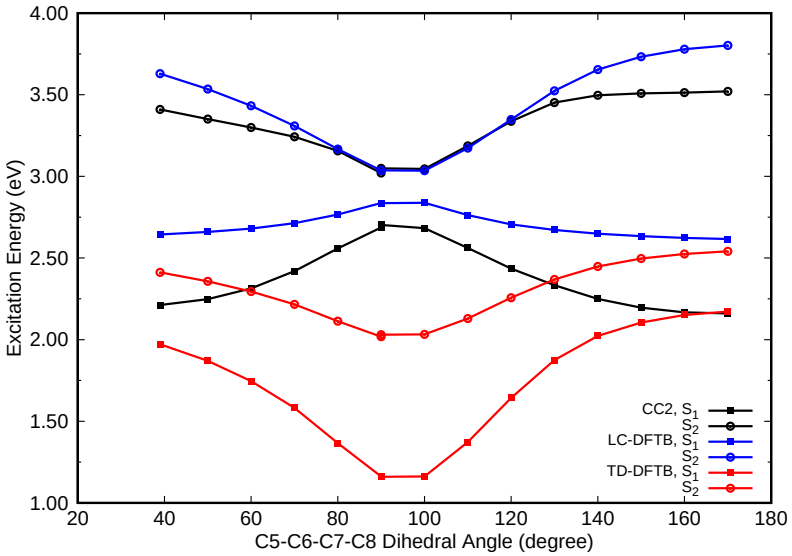

Fig. S1: Potential energy curves (S_1 and S_2) for the ground state isomerization coordinate from 6-s-cis- to 6-s-trans-PSB11. The CC2 values are taken from Ref. 10.

S-2.2. Bacteriochlorophyll a

1. Geometric and conformational impact on the absorption spectrum

Tab. S3: Excitation energies (eV) of BChl a in vacuum. Structures optimized with HF, DFT and SCC-DFTB. D1 values are given in parenthesis.

	HF	CAM-B3LYP	BH-LYP	B3LYP	DFTB	BLYP
BLA (Å)	0.102	0.032	0.019	0.005	0.004	0.004
ZINDO/S	2.137	1.568	1.512	1.466	1.458	1.445
HF/CIS	3.326	2.358	2.120	1.865	1.840	1.814
TD-DFTB	1.822	1.801	1.859	1.811	1.796	1.765
TD-BP86	2.060	2.091	2.147	2.086	2.057	2.042
TD-B3LYP	2.181	2.121	2.173	2.137	2.122	2.100
LC-DFTB*	2.369	1.906	1.934	1.865	1.848	1.811
LC-DFTB	2.398	1.908	1.926	1.853	1.833	1.800
CAM-B3LYP	2.474	2.034	2.041	1.986	1.965	1.948
LC-BLYP	2.779	2.031	1.954	1.857	1.832	1.817
ωB97X	2.826	2.048	1.967	1.867	1.843	1.826
DFT/MRCI	1.861	1.652	1.694	1.644	1.621	1.596
SOS-CC2*	2.480	1.684	1.751	1.844	1.828	1.807
	(0.1204)	(0.1959)	(0.1854)	(0.0960)	(0.0968)	(0.1150)
SOS-ADC(2)*	2.404	1.438	1.538	1.749	1.732	1.672
	(0.0577)	(0.0834)	(0.0796)	(0.0562)	(0.056)	(0.0639)

* Modified side chains.

The BLA of the optimized BChl a structure has been calculated to study the structural differences using the diaza[18]-annulene substructure as described in the main text.

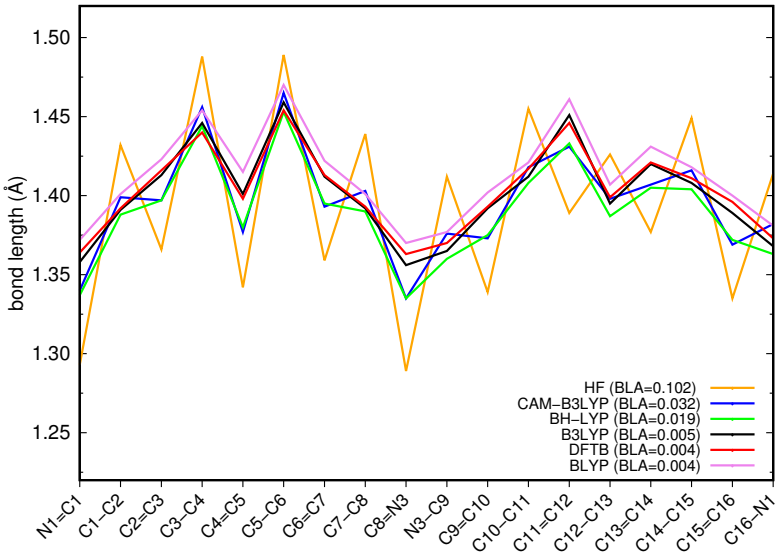

Fig. S2: Bond lengths of BChl a in vacuum obtained by different optimization methods and BLA values (Å).

In Fig. S2, the bond lengths are plotted as well as the BLA values (in Å). In contrast to all other methods, HF shows a completely different trend of the bond lengths, i.e., an alternation of the single and double bonds over the whole ring. Standard DFT functionals (B3LYP and BLYP) as well as DFTB yield less alternations reflected also by the small BLA ($\sim$ 0.004) compared to HF (0.102). In a previous study [11] it was reported already that B3LYP leads to an improved description of BChl a geometries compared to HF, which is consistent with the results here, i.e., a significant overestimation of the BLA using HF. DFTB reveals a similar BLA as B3LYP and is therefore applicable for, e.g., QM/MM MD simulations of LH complexes. The larger the amount of HF in the functional, the stronger is the alternation of bond length as seen in the case of BH-LYP (0.019) or CAM-B3LYP (0.032) showing a higher BLA than B3LYP. The optimized structures of BChl a in vacuum show a planar structure, except the one obtained using CAM-B3LYP showing a bowl shape. This bowl shape can also be found in proteins. Hence, this structure is helpful to see whether a different shape has an influence on the excitation energies, as discussed below. SOS-CC2 and SOS-ADC(2) result in a slight red shift when computing the excitation energies on this geometry, which is not found by the other methods.

2. Effect of electrostatic environment

Tab. S4: Vertical excitation energies (eV) in vacuum and with protein environment of BChl a chromophores in the FMO complex of *P. aestuarii*. Structures taken from Ref. 12.

	1	2	3	4	5	6	7
BLA (Å)	+0.006	+0.009	-0.004	+0.015	+0.017	+0.028	-0.008
vacuum							
ZINDO/S (10,10)	1.483	1.481	1.494	1.489	1.520	1.518	1.487
TD-DFTB	1.806	1.797	1.805	1.793	1.815	1.793	1.811
B3LYP	2.098	2.107	2.114	2.094	2.114	2.099	2.108
LC-DFTB	1.837	1.836	1.834	1.832	1.868	1.863	1.839
CAM-B3LYP	1.971	1.976	1.977	1.971	2.001	2.008	1.977
ωB97X	1.855	1.863	1.851	1.879	1.927	1.978	1.861
DFT/MRCI	1.647	1.636	1.642	1.633	1.645	1.633	1.634
SOS-ADC(2)	1.724	1.639	1.844	1.487	1.485	1.437	1.695
protein							
ZINDO/S (10,10)	1.482	1.474	1.504	1.511	1.587	1.829	1.491
TD-DFTB	1.756	1.755	1.784	1.764	1.806	1.796	1.778
B3LYP	2.076	2.080	2.102	2.084	2.113	2.119	2.091
LC-DFTB	1.805	1.821	1.835	1.822	1.892	1.975	1.844
CAM-B3LYP	1.960	1.972	1.978	1.977	2.034	2.138	1.983
ωB97X	1.849	1.883	1.868	1.920	2.023	2.263	1.902
DFT/MRCI	1.619	1.605	1.636	1.628	1.667	1.700	1.632
SOS-ADC(2)	1.611	1.456	1.670	1.449	1.512	1.705	1.538

Tab. S5: Shifts (protein-vacuum) of the vertical excitation energies (eV) of BChl a chromophores in the FMO complex of *P. aestuarii*. Structures taken from Ref. 12.

	1	2	3	4	5	6	7
ZINDO/S	-0.001	-0.007	+0.010	+0.022	+0.067	+0.311	+0.004
TD-DFTB	-0.050	-0.042	-0.021	-0.029	-0.009	+0.003	-0.033
B3LYP	-0.022	-0.027	-0.012	-0.010	-0.001	+0.020	-0.017
LC-DFTB	-0.032	-0.015	+0.001	-0.010	+0.024	+0.112	+0.005
CAM-B3LYP	-0.011	-0.004	+0.001	+0.006	+0.033	+0.130	+0.006
ωB97X	-0.006	+0.020	+0.017	+0.041	+0.096	+0.285	+0.041
DFT/MRCI	-0.028	-0.031	-0.006	-0.005	0.022	+0.067	-0.002
SOS-ADC(2)	-0.113	-0.183	-0.174	-0.038	0.027	+0.268	-0.157

3. Exciton coupling I: Computational Cost

The computational cost for the supermolecular calculations has to be pointed out here: Using ORCA and the LC-DFT functional CAM-B3LYP taking 6 cores in parallel, the computation time takes about 2–3 days for one BChl a dimer, while for LC-DFTB it takes only about 15 minutes on a single core. Moreover, the Coulomb couplings computed using LC-DFTB are obtained in just few seconds. This highlights the power of the LC-DFTB approach for fast computations and applications for the study of larger systems such as LH complexes.

4. Exciton coupling II: Light Harvesting Complex II (LH2) B850 ring

Tab. S6: Exciton couplings and Coulomb couplings for the respective BChl a dimers $\alpha\beta$ (V_1) and $\beta\alpha$ (V_2) of the LH2 B850 ring. The distance is measured between the respective Mg ions. The excitonic couplings have been determined using the supermolecular approach as half of the energy splitting. The partial charges of the TrESP and Tr-Mulliken values are based on CAM-B3LYP. The mean absolute error (MAE) is given in the last row with respect to the supermolecular results using the ωB97X and CAM-B3LYP functionals.

Distance	Type	Supermolecular approach			Coulomb Coupling		
(Å)		ωB97X	CAM-B3LYP	LC-DFTB	TrESP	Tr-Mulliken	LC-DFTB
9.63	V^2	0.071	0.070	0.065	0.061	0.058	0.075
9.28	V^1	0.052	0.052	0.049	0.045	0.039	0.052
9.53	V^2	0.066	0.065	0.061	0.058	0.056	0.072
8.55	V^1	0.047	0.050	0.049	0.036	0.028	0.034
9.47	V^2	0.073	0.074	0.064	0.061	0.055	0.073
8.94	V^1	0.055	0.055	0.060	0.047	0.040	0.052
9.44	V^2	0.072	0.072	0.068	0.060	0.057	0.074
9.51	V^1	0.043	0.042	0.041	0.038	0.033	0.046
9.86	V^2	0.066	0.065	0.062	0.059	0.057	0.073
8.95	V^1	0.045	0.047	0.047	0.039	0.033	0.044
9.55	V^2	0.061	0.059	0.058	0.054	0.049	0.066
9.15	V^1	0.073	0.081	0.077	0.057	0.050	0.066
9.26	V^2	0.072	0.076	0.065	0.057	0.051	0.069
8.60	V^1	0.059	0.067	0.067	0.041	0.033	0.041
9.38	V^2	0.071	0.075	0.065	0.057	0.055	0.069
8.83	V^1	0.061	0.068	0.067	0.048	0.040	0.051
MAE wrt ωB97X	-	-	0.003	0.005	0.011	0.016	0.005

Tab. S7: Previous studies on exciton couplings of LH2 complexes based on the X-ray structure. The Coulomb couplings of the most strongly coupled BChl a dimers are displayed.

		Methods		Coulomb Couplings	
Reference	X-ray Structure	Excitation Energy	Coulomb Couplings	cm^{-1}	eV
Krüger et *al.* [13] (1998)	LH2 *Rps. ac.*	CIS	TDC	238	0.03
		(3-21G*)		213	0.03
Cory et *al.* [14] (1998)	LH2 *Rs. ms.*	INDO-CIS	INDO-CIS	790	0.10
			effective Hamiltonian	369	0.05
Scholes et *al.* [15] (1999)[a]	LH2 *Rps. ac.*	CIS	CIS (6-31G*)	320	0.04
			(scaled exp.)	255	0.03
Madjet et *al.* [6] (2006)	LH2 *Rps. ac.*	CIS,	TrESP, CIS	245	0.03
		TD-DFT/B3LYP	TrESP,TD-DFT/B3LYP	211	0.03
		(6-31G*)			
Neugebauer [16] (2008)	LH2 *Rps. ac.*	TD-DFT +FDE	supermol. TD-DFT + FDE	242	0.03
		(SOAP/TZP)	supermol. TD-DFT[b]	252	0.03
			FDEc	232	0.03
				200	0.02
Cupellini et *al.* [17] (2016)	LH2 *Rps. ac.*	TD-DFT + MMPOL,	TD-DFT + MMPOL	409	0.05
		CAM-B3LYP (6-31G(d))	by EXAT[c]	362	0.04
Segatta et *al.* [18] (2017)	LH2 *Rps. ac.*	RASSCF/RASPT2	TDC[c]	563	0.07
				474	0.06
		TD-DFT + MMPol	TD-DFT + MMPol	336	0.04
		CAM-B3LYP		288	0.04

[a]also performed supermol. calc. CIS(6-31G*): 0.09 eV (730 cm^{-1}) and 0.07 eV (550 cm^{-1}); [b]DFT E_{xc} functional of GGA type: exchange by Becke, and correlation functional by PW91 [16]; [c]used program EXAT for computing the excitonic Hamiltonian [17, 19]; [d]no explicit screening factor used

Tab. S8: Previous studies on Coulomb couplings of LH2 complexes computed on sampled structures along classical MD trajectories. Values of the most strongly coupled BChl a dimers are displayed.

		Methods		Coulomb Couplings	
Reference	X-Ray Structure, MD	Excitation Energy	Coulomb Coupling	cm^{-1}	eV
Olbrich et *al.* [7] (2011)	LH2 *Rs. ms.*, 12 ps	ZINDO/S-CIS	PDA[a]	274	0.03
			TrESP, TD-DFT/B3LYP	173	0.02
				140	0.02
Cupellini et *al.* [17] (2016)	LH2 *Rps. ac.*, 100ns	TD-DFT + MMPol,	TD-DFT + MMPol	339	0.04
		CAM-B3LYP (6-31G(d))	by EXAT[b]	317	0.04

[a] transition densities obtained by ZINDO/S-CIS

[b] EXAT is the program used for computing the excitonic Hamiltonian, cf. Ref. [17, 19]

S-3. PERFORMANCE OF LC-DFTB ON BIOLOGICAL MODEL SYSTEMS

S-3.1. Rhodopsins

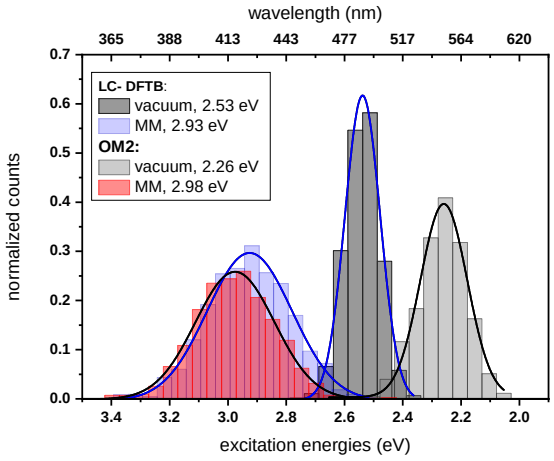

Fig. S3: Simulated absorption spectrum of ppR. LC-DFTB and OM2/MRCI have been used for the computation of the excitation energies. The histograms are based on snapshot geometries of the 1 ns-long QM/MM MD trajectories. Plotted are the excitation energies weighted by the oscillator strength for (i) only the retinal chromophore (vacuum) and (ii) with additional fixed MM point charges to account for the protein environment (MM). Gaussian functions are used to determine the corresponding maxima, in blue: LC-DFTB and in black: OM2/MRCI.

S-3.2. Light-harvesting complexes

1. LH2 complex of Rs. molischianum, QM/MM optimized model

Tab. S9: BLA (Å), vacuum excitation energies (eV) and the resulting shifts (eV, protein-vacuum) have been determined of the B800 of LH2 from *Rhodospirillum (Rs.) molischianum*. The excitation energies have been calculated using LC-DFTB and ZINDO/S based on the DFTB QM/MM optimized model.

		LC-DFTB			ZINDO/S		
BChl	BLA	vacuum	protein	shift	vacuum	protein	shift
1	0.010	1.827	1.839	+0.012	1.458	1.522	+0.064
2	0.013	1.836	1.888	+0.052	1.463	1.604	+0.141
3	0.006	1.823	1.857	+0.034	1.456	1.571	+0.115
4	0.007	1.828	1.811	-0.017	1.461	1.442	-0.019
5	0.014	1.842	1.841	-0.001	1.471	1.465	-0.006
6	0.010	1.822	1.796	-0.026	1.453	1.428	-0.025
7	0.011	1.822	1.828	+0.006	1.456	1.485	+0.029
8	0.011	1.830	1.834	+0.004	1.465	1.481	+0.016

Tab. S10: Same as in Tab. S9, but for the B850 ring.

		LC-DFTB			ZINDO/S		
BChl	BLA	vacuum	protein	shift	vacuum	protein	shift
1	0.005	1.828	1.846	+0.018	1.457	1.498	+0.041
2	0.001	1.827	1.827	+0.000	1.454	1.454	+0.000
3	0.008	1.833	1.836	+0.003	1.463	1.474	+0.011
4	0.003	1.826	1.821	-0.005	1.452	1.460	+0.008
5	0.007	1.826	1.835	+0.009	1.456	1.473	+0.017
6	0.004	1.831	1.826	-0.005	1.456	1.464	+0.008
7	0.003	1.833	1.832	-0.001	1.458	1.461	+0.003
8	0.003	1.822	1.812	-0.010	1.448	1.444	-0.004
9	0.005	1.826	1.824	-0.002	1.457	1.466	+0.009
10	0.005	1.831	1.842	+0.011	1.453	1.461	+0.008
11	0.005	1.833	1.848	+0.015	1.460	1.517	+0.057
12	0.002	1.826	1.820	-0.006	1.449	1.447	-0.002
13	0.005	1.833	1.818	-0.015	1.461	1.455	-0.006
14	0.004	1.828	1.818	-0.010	1.449	1.440	-0.009
15	0.005	1.834	1.825	-0.009	1.459	1.461	+0.002
16	0.002	1.820	1.820	+0.000	1.446	1.470	+0.024

Tab. S11: Average excitation energies and variances (eV) based on DFTB QM/MM optimized BChl a structures of the B800 and the B850 ring systems of LH2 from *Rs. molischianum*. Shown are the excitation energies for the individual BChl a chromophores with and without the influence of the protein environment. Moreover, the excitonic energies (eV), i.e., the lowest eigenvalues are shown for the ring systems. The excitation energies have been computed using ZINDO/S, Coulomb couplings with LC-DFTB and TrESP.

	B800	B850	B850 shift
vacuum[a]	1.460 ± 0.006	1.455 ± 0.005	–0.005
protein[a]	1.500 ± 0.062	1.465 ± 0.019	–0.035
ring system			
LC-DFTB	1.427	1.372	–0.055
TrESP	1.427	1.358	–0.069
Experimental [20]			–0.085

[a] BChl a monomer

2. LH2 complex, classical MD simulations

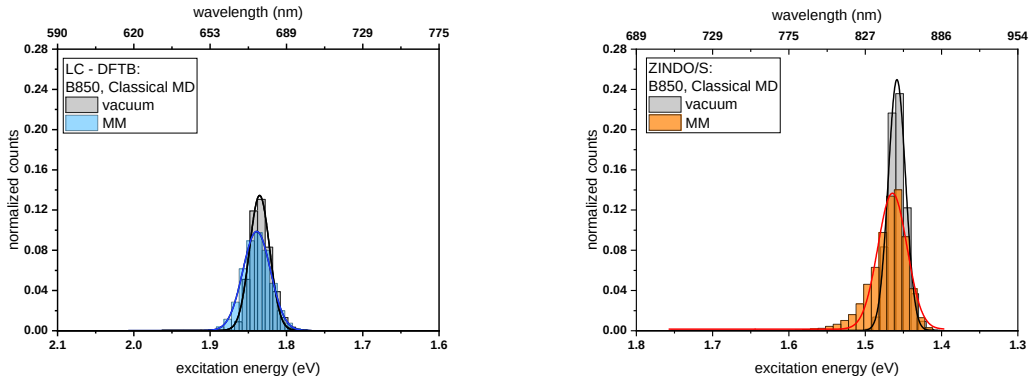

(a) (b)

Fig. S4: Simulated absorption spectrum of the B850 ring of LH2 from *Rs. molischianum*. (a) LC-DFTB has been used for the computation of the excitation energies; (b) ZINDO/S has been used for the computation of the excitation energies. All histograms are based on snapshot geometries along a classical MD trajectory of 1 ns length. Plotted are the excitation energies weighted by the oscillator strength for (i) only the BChl a chromophore (vacuum) and (ii) with additional fixed MM point charges to account for the protein environment (MM). Gaussian functions have been used to determine the corresponding maxima.

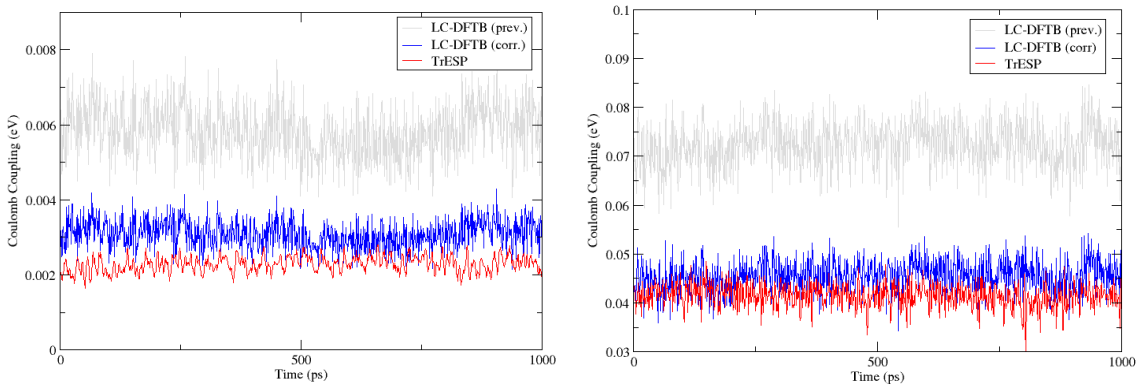

(a) (b)

Fig. S5: Coulomb couplings sampled along a classical MD trajectory of 1 ns length for (a) one BChl a dimer pair with the strongest Coulomb couplings chosen as example for the B800 ring and for (b) one BChl a dimer pair with the strongest Coulomb couplings chosen as example for the B850 ring.

Tab. S12: Average excitation energies and standard deviations (eV) based on sampled structures along a classical MD trajectory of LH2 from *Rs. molischianum*. Shown are the excitation energies for the individual BChl a chromophores with and without the influence of the protein environment. The average excitation energies are obtained by averaging the maxima of Gaussian fits to the distributions of the respective chromophores. In addition, excitonic energies (eV), i.e., the lowest eigenvalues are shown for the complete ring systems. The excitonic energies have been obtained by the maxima of Gaussian fits to the distributions of the exciton energies, respectively. The excitation energies have been computed using ZINDO/S, Coulomb couplings using LC-DFTB and TrESP.

	B800	B850	B850 shift
vacuum[a]	1.462 ± 0.002	1.458 ± 0.004	–0.004
protein[a]	1.480 ± 0.008	1.466 ± 0.010	–0.014
ring system			
LC-DFTB	1.449	1.367	–0.082
TrESP	1.451	1.401	–0.050
Experimental [20]			–0.085

[a]BChl a monomer

Tab. S13: Excitonic energies (eV) of LH2 from *Rs. molischianum* on the LC-DFTB level of theory obtained for the DFTB QM/MM optimized model and sampled along an MD trajectory.

Excitonic energy	QM/MM optimized	classical MD
B800		
E_1	1.794	1.815
E_2	1.809	1.828
E_3	1.824	1.837
E_4	1.833	1.845
E_5	1.843	1.853
E_6	1.844	1.862
E_7	1.857	1.873
E_8	1.890	1.891
B850		
E_1	1.730	1.737
$E_{2,3}$	1.733, 1.738	1.746, 1.752
$E_{4,5}$	1.746, 1.748	1.759, 1.766
$E_{6,7}$	1.758, 1.765	1.774, 1.782
E_8	1.773	1,792
E_9	1.820	1,838
$E_{10,11}$	1.848, 1.849	1.861, 1.870
$E_{12,13}$	1.898, 1.908	1.914, 1.923
$E_{14,15}$	1.965, 1.968	1.975, 1.985
E_{16}	2.004	2.018

Tab. S14: Excitonic energy range (eV) dependent how the averaged values are computed, of the QM/MM optimized model and the structures sampled along the MD trajectory of LH2 from *Rs. molischianum*. LC-DFTB and ZINDO/S have been used for the computations of the excitation energies. The Coulomb couplings have been calculated using LC-DFTB and TrESP. Values obtained by averaging firstly the hamiltonians are given in parenthesis.

		QM/MM optimized	classical MD
B800			
Excitation energy	Coulomb coupling		
LC-DFTB	LC-DFTB	0.096	0.076 (0.030)
	TrESP	0.094	0.072 (0.024)
ZINDO/S	LC-DFTB	0.179	0.137 (0.034)
	TrESP	0.178	0.134 (0.029)
B850			
LC-DFTB	LC-DFTB	0.274	0.281 (0.265)
	TrESP	0.227	0.163 (0.147)
ZINDO/S	LC-DFTB	0.284	0.288 (0.265)
	TrESP	0.238	0.175 (0.147)

3. LH2 complex Rs. molischianum vs. Rps. acidophila

Tab. S15: Average excitation energies and standard deviations (eV) based on DFTB QM/MM optimized BChl a structures of the B800 and the B850 ring systems sampled along a MD trajectory of LH2 from *Rps. acidophila*. Shown are the excitation energies for the individual BChl a chromophores with and without the influence of the protein environment. Moreover, excitonic energies (eV), i.e. the lowest eigenvalues are shown for the complete ring system. Excitation energies have been computed using LC-DFTB, Coulomb couplings using LC-DFTB and TrESP.

	B800	B850	B850 shift
QM/MM optimized			
vacuum[a]	1.845 ± 0.004	1.818 ± 0.002	–0.027
protein[a]	1.844 ± 0.012	1.813 ± 0.004	–0.031
ring system	1.802	1.707	–0.095
	1.811	1.714	–0.097[b]
classical MD			
vacuum[a]	1.838 ± 0.002	1.828 ± 0.002	–0.010
protein[a]	1.837 ± 0.004	1.827 ± 0.004	–0.010
ring system	1.799	1.718	–0.081
	1.814	1.726	–0.088[b]
Experimental[21], low temperature (1.2K, 5K)			–0.116
Experimental[21], room temperature			–0.102

[a]BChl a monomer; [b]second lowest excitonic energy value

The LH2 complexes of *Rps. acidophila* and *Rs. molischianum* are different, e.g., in the number of chromophores or the distances between the chromophores. Although the main absorption maxima are in the same range, i.e., the rings are both called B800 and B850, they differ slightly in the absorption spectra as has been shown in previous studies [20, 22, 23].

The computation of both models using LC-DFTB shows differences in the excitation energy as well as excitonic energy ranges, especially for the B800 ring when using the DFTB QM/MM optimized models. The excitation energy range in vacuum is about twice as

large for both ring systems of the LH2 complex *Rps. acidophila* compared to the LH2 complex *Rs. molischianum*. This indicates, that the BChl a geometries are differently modified through the respective protein environment. This is reflected also in the resulting energy shift between the rings, since the LH2 complex of *Rps. acidophila* shows an vacuum energy shift of 0.027 eV between both rings, while no shift is obtained for the LH2 complex of *Rs. molischianum*. In both proteins the inclusion of the protein environment has minor effects, see Tab. S15, i.e., the shifts increase only slightly. Differences are also found in the Coulomb coupling values of the B800 ring of *Rps. acidophila*, which are larger (0.007-0.010 eV) than in LH2 of *Rs. molischianum* (0.006 eV), since the BChl a chromophores are arranged slightly more close.

The structures from the MD trajectories, show a decrease of the differences between both LH2 complexes compared to the QM/MM optimized model, as shown in the figures in the main text (Sec. 4.2.1). This indicates, that the QM/MM optimized models obtain local minima, while sampling improves the description, as discussed in the main text. The resulting energy shifts of B800-B850 considering the sampled Hamiltonian is larger for LH2 of *Rps. acidophila* (0.081 eV) than for LH2 of *Rs. molischianum* (0.078 eV). This is qualitatively in agreement with experimental results, suggesting a slightly larger energy gap of LH2 of *Rps. acidophila* [20–23]

Cupellini et al. [17] investigated the LH2 complex *Rps. acidophila*, whose work differs in several aspects from ours: (i) we use a DFTB QM/MM optimized model instead of the crystal structures, which could lead to deviations in the results, due to the missed lipid membrane and water environment; (ii) Cupellini et al. [17] made use of symmetry and considered only one BChl a chromophore of each type, i.e., one α, β, γ- BChl a chromophore. The geometry optimization of all chromophores breaks this symmetry which was there by construction of the system and leads to more static disorder, i.e., to a larger spread in the diagonal Hamiltonian matrix elements; (iii) to compute the Coulomb couplings, Cupellini et al. [17] used CAM-B3LYP, which leads to similar values as LC-DFTB as shown in Sec. 3.2.4, main text. The LC-DFTB Coulomb approximation, however, tends to increase the values slightly. Further, Cupellini et al. [17] employed a polarizable embedding scheme decreasing the couplings slightly. In the case of the B800 ring Cupellini et al. [17] find a splitting of 0.03 eV considering the lowest and the highest excitonic energy, while we find a splitting of about 0.09 eV using LC-DFTB and TrESP. This mainly results from the diagonal disorder,

since the couplings do not contribute much. For the B850 ring, they report a splitting of 0.205 eV, while LC-DFTB yields 0.274 eV and TrESP 0.227 eV. Here, the diagonal disorder is less important, and the main difference stems from the different couplings. However, the absolute value of the B850 splitting is overestimated independent of the used excitonic state as discussed in Ref. 17 by all computational approaches when compared to the experimental value of 0.179 eV at low temperatures [24].

Tab. S16: Excitonic energies (eV) of LH2 *Rps. acidophila* using LC-DFTB for both, i.e. excitation energies and Coulomb couplings. Data are given for the QM/MM optimized model and for sampled structures along a MD trajectory.

Excitonic energy	QM/MM optimized	classical MD
B800		
E_1	1.802	1.799
E_2	1.811	1.814
E_3	1.826	1.823
E_4	1.832	1.832
E_5	1.838	1.841
E_6	1.849	1.850
E_7	1.852	1.859
E_8	1.867	1.869
E_9	1.923	1.882
E_9–E_1	0.121	0.083
B850		
E_1	1.707	1.718
$E_{2,3}$	1.714, 1.717	1.726, 1.731
$E_{4,5}$	1.725, 1.728	1.737, 1.742
$E_{6,7}$	1,735, 1.738	1.749, 1,755
$E_{8,9}$	1.744, 1.752	1.763, 1.771
$E_{10,11}$	1.813, 1.818	1.831, 1.839
$E_{12,13}$	1.850, 1.855	1.868, 1.876
$E_{14,15}$	1.903, 1.910	1.922, 1.930
$E_{16,17}$	1.962, 1.966	1.979, 1.987
E_{18}	1.998	2.017
E_{18}–E_1	0.291	0.299

4. FMO complex, QM/MM optimized structure

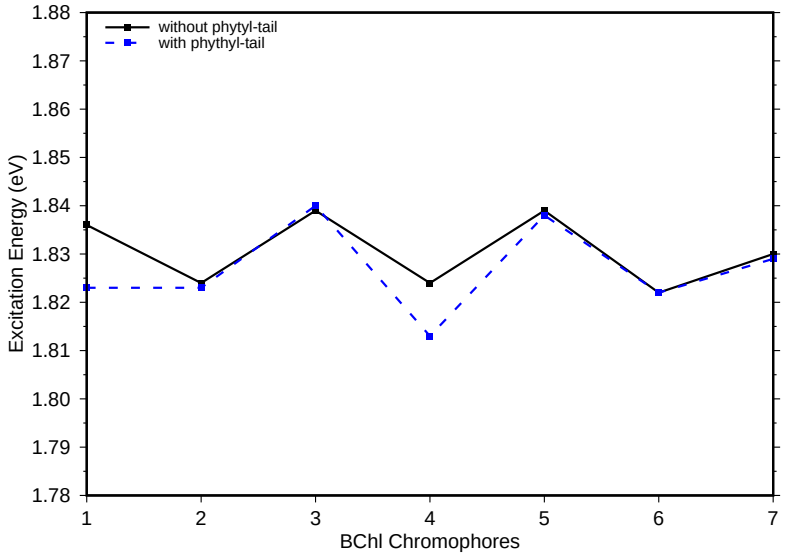

Fig. S6: Excitation energies (eV) in vacuum of the seven BChl a chromophores from FMO with and without the phythyl tail computed using LC-DFTB.

Differences are found in the vacuum excitation energies for chromophore 1 and 4, when considering the complete BChl a chromophore, i.e. with the phythyl tail. These differences lead to a red shift for both chromophores and are in agreement with a previous study [25].

Tab. S17: Coulomb couplings (eV) between all BChl a chromophores in the FMO complex using LC-DFTB. Monomer excitation energies using LC-DFTB are given on the diagonal and the strongest couplings in bold (only the new values are shown).

H_{mn}	1	2	3	4	5	6	7
1	1.701	**0.022**	0.001	0.001	0.001	0.001	0.000
2	**0.022**	1.676	**0.009**	0.002	0.001	0.003	0.002
3	0.001	**0.009**	1.710	**0.011**	0.001	0.002	0.000
4	0.001	0.002	**0.011**	1.680	**0.021**	0.005	**0.009**
5	0.001	0.001	0.001	**0.021**	1.702	**0.019**	0.001
6	0.001	0.003	0.002	0.005	**0.019**	1.670	**0.014**
7	0.000	0.002	0.000	**0.009**	0.001	**0.014**	1.729

Tab. S18: Maximum and minimum of excitation energy and excitonic energy of the DFTB QM/MM optimized BChl a chromophores of the FMO complex. ZINDO/S is used for the computation of excitation energies without (vacuum) and with the protein environment as fixed MM point charges. Coulomb couplings are computed using LC-DFTB and TrESP.

	Max	Min	shift
vacuum[a]	1.486	1.452	–0.034
protein[a]	1.544	1.451	–0.093
coupled chromophores			
LC-DFTB	1.567	1.408	–0.159
TrESP	1.553	1.428	–0.125
Experimental[26]	1.563	1.503	–0.060

[a]BChl a monomer

5. FMO complex, classical MD simulation

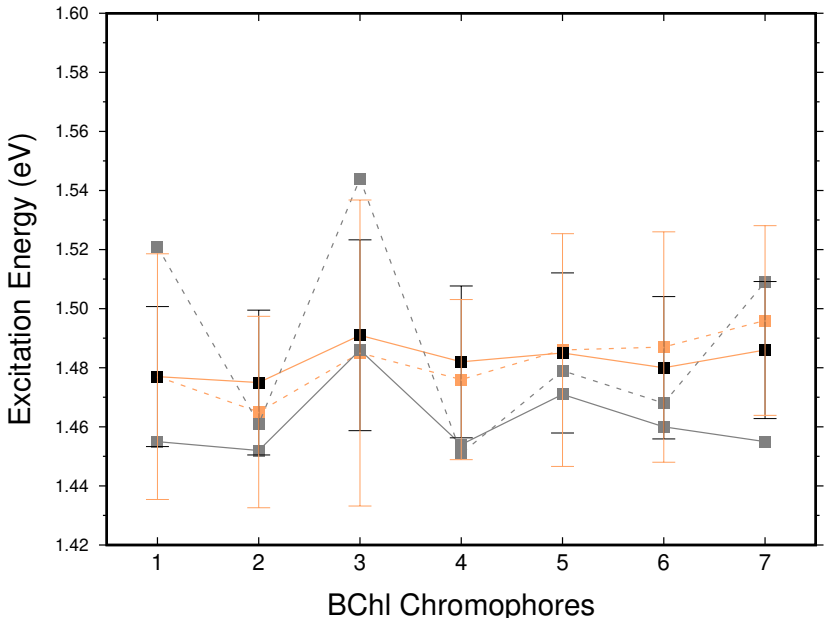

Fig. S7: Excitation energies (eV) of the FMO complex of the seven BChl a chromophores of the DFTB QM/MM optimized model and maxima of the Gaussian distributions of the classical MD sampled structures; calculated in vacuum and with fixed MM point charges using ZINDO/S.

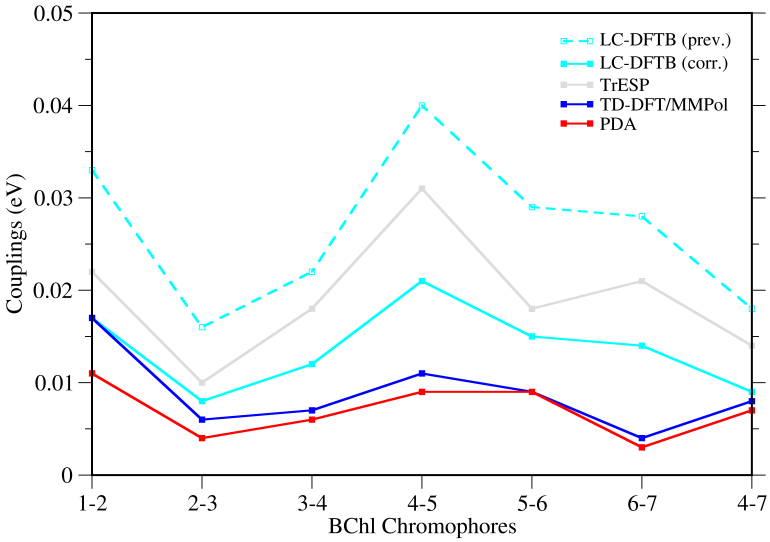

Fig. S8: Coulomb couplings (eV) averaged along a classical MD trajectory. The values for TD-DFT/MMPol have been taken from Ref. 25 and the values of PDA from Ref. 27.

The Coulomb couplings averaged along a classical MD trajectory are shown in Fig. S8. LC-DFTB shows qualitatively the same trend as TrESP. As expected from the results presented in the benchmark study in the main text (Sec. 3.2.3 and 3.2.4), LC-DFTB overestimates the Coulomb couplings. Both LC-DFTB and TrESP display qualitatively the same trend as the Coulomb couplings obtained using TD-DFT/MMPol [25] and PDA [27] in previous studies. Differences are only found for the BChl a dimer 6-7, where the values increased from dimer 5-6 to dimer 6-7. One reason might be the different FMO complex in the case of Ref. [25] using the FMO complex of *P. aestuarii* while in the case of Ref. [27] the trimer of the FMO complex *C. tepidum* has been used.

Tab. S19: Strongest Coulomb couplings (eV) computed using LC-DFTB for the DFTB QM/MM optimized model of BChl a dimers and average Coulomb couplings as maxima of Gaussian fits of the MD sampled structures.

BChl a dimer	QM/MM optimized	Classical MD
1-2	**0.022** (0.044)	**0.017** ± **0.003** (0.033 ± 0.006)
2-3	**0.009** (0.019)	**0.008** ± **0.001** (0.016 ± 0.001)
3-4	**0.011** (0.021)	**0.012** ± **0.003** (0.022 ± 0.006)
4-5	**0.021** (0.043)	**0.021** ± **0.003** (0.040 ± 0.005)
5-6	**0.019** (0.037)	**0.015** ± **0.003** (0.029 ± 0.007)
6-7	**0.014** (0.028)	**0.014** ± **0.003** (0.028 ± 0.005)
7-4	**0.009** (0.019)	**0.009** ± **0.003** (0.018 ± 0.006)

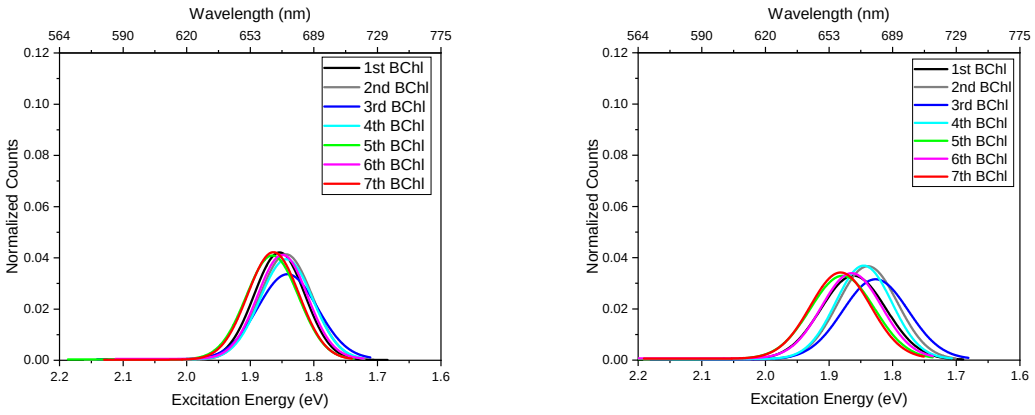

(a) (b)

Fig. S9: Excitation energies (eV) of the sampled BChl a chromophores of the FMO complex using LC-DFTB. (a) vacuum; (b) with fixed MM point charges.

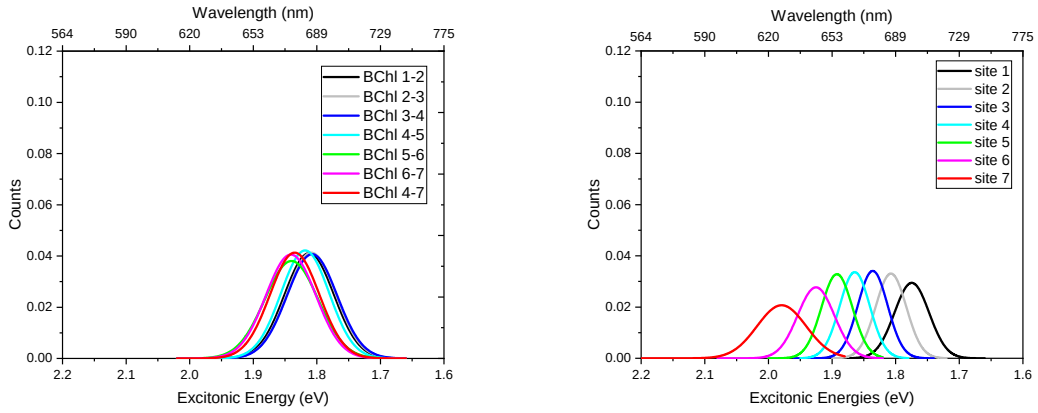

(a) (b)

Fig. S10: Excitonic energies (eV) of the sampled BChl a chromophores of the FMO complex using LC-DFTB. (a) BChl a dimers; (b) fully coupled system.

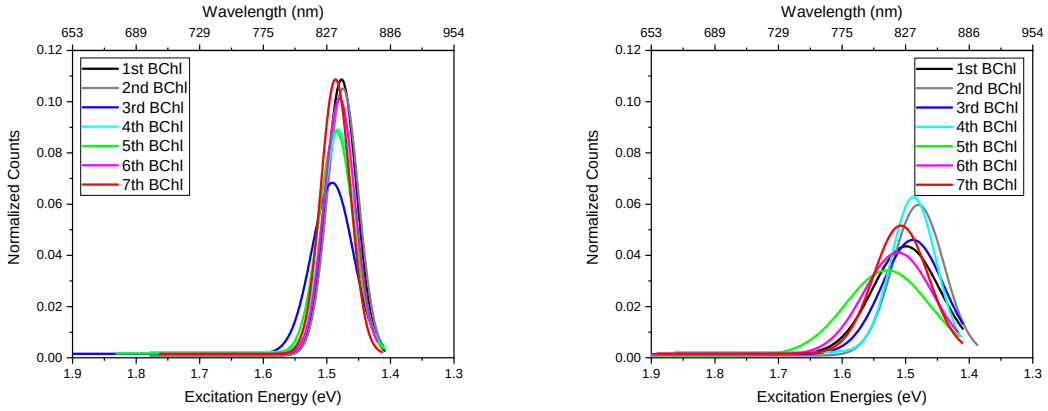

(a) (b)

Fig. S11: Excitation energies (eV) of the sampled BChl a chromophores of the FMO complex using ZINDO/S. (a) vacuum; (b) with fixed MM point charges.

Non-Gaussian energy distribution are obtained when using ZINDO/S. This behavior was already reported in a previous study concerning the trimer of the FMO complex using ZINDO/S for the excitation energies [7, 28].

Tab. S20: Maximum and minimum excitation and excitonic energies of the structures along a MD simulation of the FMO complex. ZINDO/S is used for the computation of the excitation energies without (vacuum) and with the protein environment as fixed point charges. The Coulomb couplings have been computed using LC-DFTB and TrESP.

	Max	Min	shift
vacuum	1.491	1.475	-0.016
protein	**1.496** (1.529)	**1.465** (1.480)	**-0.031** (-0.049)
coupled chromophores			
LC-DFTB	**1.618** (1.657)	**1.441** (1.436)	**-0.177** (-0.221)
TrESP	1.648	1.446	-0.202
Experimental	1.563	1.503	-0.060

Tab. S21: Excitonic energies (eV) of the FMO complex from *C. tepidum* based on the QM/MM optimized structures and averaged along a MD trajectory. The excitation energies and the Coulomb couplings have been computed using LC-DFTB.

QM/MM optimized	MD simulation
1.656 (1.756)	**1.659** (1.775)
1.662 (1.767)	**1.686** (1.807)
1.670 (1.790)	**1.707** (1.836)
1.707 (1.833)	**1.726** (1.864)
1.714 (1.848)	**1.749** (1.892)
1.721 (1.864)	**1.774** (1.925)
1.738 (1.899)	**1.811** (1.979)

[1] W. G. Hoover, Phys. Rev. A, 1985, **31**, 1695–1697.

[2] S. Nosé, Mol. Phys., 1984, **52**, 255–268.

[3] M. Parrinello and A. Rahman, J. Appl. Phys., 1981, **52**, 7182–7190.

[4] V. Stehr, R. F. Fink, B. Engels, J. Pflaum and C. Deibel, J. Chem. Theory Comput., 2014,

10, 1242–1255.

[5] E. P. Kenny and I. Kassal, J. Phys. Chem. B, 2016, **120**, 25–32.

[6] M. E. Madjet, A. Abdurahman and T. Renger, J. Phys. Chem. B, 2006, **110**, 17268–17281.

[7] C. Olbrich, T. L. C. Jansen, J. Liebers, M. Aghtar, J. Strümpfer, K. Schulten, J. Knoester and U. Kleinekathöfer, J. Phys. Chem. B, 2011, **115**, 8609–8621.

[8] J. J. Kranz and M. Elstner, J. Chem. Theory Comput., 2016, **12**, 4209–4221.

[9] M. Wanko, M. Hoffmann, P. Strodel, A. Koslowski, W. Thiel, F. Neese, T. Frauenheim and M. Elstner, J. Phys. Chem. B, 2005, **109**, 3606–3615.

[10] A. Dwyer, Ph.D. thesis, Durham University, 2011.

[11] J. Linnanto and J. Korppi-Tommola, Phys. Chem. Chem. Phys., 2006, **8**, 663–687.

[12] N. H. List, C. Curutchet, S. Knecht, B. Mennucci and J. Kongsted, J. Chem. Theory Comput., 2013, **9**, 4928–4938.

[13] B. P. Krueger, G. D. Scholes and G. R. Fleming, J. Phys. Chem. B, 1998, **102**, 5378–5386.

[14] M. G. Cory, M. C. Zerner, X. Hu and K. Schulten, J. Phys. Chem. B, 1998, **102**, 7640–7650.

[15] G. D. Scholes, I. R. Gould, R. J. Cogdell and G. R. Fleming, J. Phys. Chem. B, 1999, **103**, 2543–2553.

[16] J. Neugebauer, J. Phys. Chem. B, 2008, **112**, 2207–2217.

[17] L. Cupellini, S. Jurinovich, M. Campetella, S. Caprasecca, C. a. Guido, S. M. Kelly, A. T. Gardiner, R. Cogdell and B. Mennucci, J. Phys. Chem. B, 2016, **120**, 11348–11359.

[18] F. Segatta, L. Cupellini, S. Jurinovich, S. Mukamel, M. Dapor, S. Taioli, M. Garavelli and B. Mennucci, J. Am. Chem. Soc., 2017, **139**, 7558–7567.

[19] S. Jurinovich, L. Cupellini, C. A. Guido and B. Mennucci, J. Comput. Chem., 2018, **39**, 279–286.

[20] J.-p. Zhang, R. Fujii, P. Qian, T. Inaba, T. Mizoguchi, Y. Koyama, K. Onaka, Y. Watanabe and H. Nagae, J. Phys. Chem. B, 2000, **104**, 3683–3691.

[21] R. Kunz, K. Timpmann, J. Southall, R. J. Cogdell, J. Köhler and A. Freiberg, J. Phys. Chem. B, 2013, **117**, 12020–12029.

[22] S. Georgakopoulou, R. N. Frese, E. Johnson, C. Koolhaas, R. J. Cogdell, R. Van Grondelle and G. Van Der Zwan, Biophys. J., 2002, **82**, 2184–2197.

[23] M. I. Mallus, Y. Shakya, J. D. Prajapati and U. Kleinekathöfer, Chemical Physics, 2018, **515**, 141–151.

[24] M. Pajusalu, M. Rätsep, G. Trinkunas and A. Freiberg, ChemPhysChem, 2011, **12**, 634–644.

[25] S. Jurinovich, C. Curutchet and B. Mennucci, ChemPhysChem, 2014, **15**, 3194–3204.

[26] D. Hayes and G. S. Engel, Biophys. J., 2011, **100**, 2043–2052.

[27] X. Jia, Y. Mei, J. Z. H. Zhang and Y. Mo, Sci. Rep., 2015, **5**, 1–10.

[28] S. Chandrasekaran, M. Aghtar, S. Valleau, A. Aspuru-Guzik and U. Kleinekathöfer, J. Phys. Chem. B, 2015, **119**, 9995–10004.